Extended profiles with morphological attribute filters for the analysis of hyperspectral data

MAURO DALLA MURA*†‡, JON ATLI BENEDIKTSSON‡, BJÖRN WASKE§
and LORENZO BRUZZONE†

†Department of Information Engineering and Computer Science, University of Trento
Via Sommarive, 14 I-38123, Povo, Trento, Italy
‡Faculty of Electrical and Computer Engineering, University of Iceland, Hjardarhaga 2-6,
101 Reykjavik, Iceland
§Institute of Geodesy and Geoinformation, Department of Photogrammetry, University
of Bonn, Nussallee 15, 53115 Bonn, Germany

Extended attribute profiles and extended multi-attribute profiles are presented for
the analysis of hyperspectral high-resolution images. These extended profiles are
based on morphological attribute filters and, through a multi-level analysis, are
capable of extracting spatial features that can better model the spatial information,
with respect to conventional extended morphological profiles. The features
extracted by the proposed extended profiles were considered for a classification
task. Two hyperspectral high-resolution datasets acquired for the city of Pavia,
Italy, were considered in the analysis. The effectiveness of the introduced operators
in modelling the spatial information was proved by the higher classification
accuracies obtained with respect to those achieved by a conventional extended
morphological profile.

1. Introduction

Spatial information is of fundamental importance when analysing remote-sensing
images of high geometrical resolution (HR). In fact, owing to the high spatial resolu-
tion, the geometrical features of the structures in a scene have a great perceptual
significance that can be directly exploited for modelling the objects in the scene
(especially useful for object detection and extraction). This can also increase the
discriminability between different thematic classes (e.g. in classification tasks).

Several approaches can be considered for including the spatial features in the image
analysis. Pesaresi and Benediktsson (2001) presented the morphological profiles
(MPs), a multi-scale decomposition of an image carried out with opening and closing
transformations based on the geodesic reconstruction. The opening and closing
operators are defined in the mathematical morphology framework (Soille 2003).
The MP proved its effectiveness in extracting features that can model the spatial
information and was successfully employed in classification of high-resolution pan-
chromatic IKONOS images. From the concept of the MP, the derivative of the
morphological profile (DMP) was also defined in Pesaresi and Benediktsson (2001).
A DMP contains the same information as the MP, but it can be useful for visual
inspection of the scene since it shows the differences between adjacent levels of the MP
profile by enhancing the residual between subsequent filterings. From the DMP, it is

---

*Corresponding author. Email: dallamura@disi.unitn.it

possible to extract the morphological characteristic of the image that is defined as the level, for each pixel, where the absolute maximum in the DMP occurs (Pesaresi and Benediktsson 2001). Zhu *et al.* (2005) employed the morphological characteristic for extracting the road network from a high-resolution image. In Benediktsson *et al.* (2003), the increase in the dimensionality due to the computation of the MP (especially for a fine multi-scale analysis) was addressed by reducing the number of features through feature-extraction techniques (e.g. decision-boundary feature extraction, DBFE, and non-parametric weighted feature extraction, NWFE). Recently, we proposed (Dalla Mura *et al.* 2009) the use of morphological attribute filters (Breen and Jones 1996) for the classification of very-high-resolution images. In Dalla Mura *et al.* (2010), we presented attribute profiles (APs) and their derivatives (DAPs) as an extension of MPs and DMPs based on attribute filters. APs permit the modelling of the spatial information more precisely with respect to MPs, as the input image can be processed according to many attributes, which can be defined with great flexibility.

When dealing with hyperspectral data, the spectral values of the pixels carry important information, and it must be taken into account in the data analysis. For a review of the main techniques for hyperspectral image processing, we refer the reader to Plaza *et al.* (2009). The extension of mathematical morphology tools (e.g. MPs) to multi-valued data is not straightforward since an ordering relation between the elements of this set of data is not natively defined (i.e. there is no ordering relation between vectors). Benediktsson *et al.* (2005) addressed this issue by reducing the original dimensionality of the hyperspectral data by computing the MP on each of the first principal components (i.e. scalar images) extracted from the data by principal-component analysis (PCA). The concatenation of the MPs computed on the extracted features in a single structure led to the definition of the extended morphological profile (EMP). Instead of the PCA, Palmason *et al.* (2005) considered the independent-component analysis technique for future reduction. The features generated by the EMP were analysed for classification by neural networks in Benediktsson *et al.* (2005), random forests (RF) in Joelsson *et al.* (2005) and support vector machine classifiers in Fauvel *et al.* (2008). In the latter work, the EMP was considered, along with the full spectral information. Another approach for extending the concept of MPs to hyperspectral data was proposed by Plaza *et al.* (2005). According to the definition of a reduced-vector ordering scheme based on the spectral purity of pixel vectors (Plaza *et al.* 2002), an alternative version of the extended morphological profile was presented.

In this paper, we propose the definition of the extended attribute profile (EAP) and the extended multi-attribute profile (EMAP), which rely on the application of the APs to hyperspectral data and to a straightforward further extension to a multi-attribute scenario, respectively. The proposed operators can also be considered as an extension of EMPs since an AP includes in its definition the MP. The proposed techniques were applied to the classification of two high-resolution hyperspectral datasets acquired on the city of Pavia, Italy. The morphological features extracted were classified by an RF classifier.

The paper is organized into five sections. Section 2 recalls some concepts related to morphological operators and the definition of an EMP. Section 3 presents the proposed EAP and EMAP. The experimental results are presented and discussed in §4. Finally, the conclusions are drawn in §5.

2. Extended morphological profiles

This section aims at giving a brief overview on the main concepts involved in the computation of the extended profiles. For a comprehensive treatise on mathematical morphology, we refer the reader to Serra (1983), Serra (1988) and Soille (2003). The section ends by recalling the definition of the EMP.

2.1 *Mathematical morphology*

EMPs are based on the application of the morphological operators of opening and closing by reconstruction. Opening by reconstruction is an image transformation that is increasing, idempotent and anti-extensive (Salembier and Serra 1995). The degree of processing of the input image depends on the geometrical characteristics of the sliding window, called the structuring element (SE), considered in the transformation. An opening by reconstruction processes the image by removing from a scalar image all those bright (with respect to the grey-level of the neighbouring regions) connected components on which the SE does not fit in. This operator is particularly suitable for processing HR images because it does not distort the edges of the regions, but only transforms the image by merging flat regions. This leads to a reduction of the complexity of the image (according to the SE used), while preserving the geometrical characteristics of the structures not removed from the image. By duality, a closing by reconstruction processes the input image by removing dark connected components from the scene. The definitions of opening, γ_R, and closing by reconstruction, ϕ_R, of a grey-level image f, are respectively given by:

$$\gamma_R^i(f) = R_f^\delta(\varepsilon^i(f)), \tag{1}$$

$$\phi_R^i(f) = R_f^\varepsilon(\delta^i(f)), \tag{2}$$

where ε^i and δ^i are the erosion and dilation with a SE of size i, respectively, and R_f^δ and R_f^ε are the geodesic reconstruction by dilation and erosion, respectively (Soille 2003).

A morphological profile is a concatenation of a closing profile, Π_ϕ, and opening profile, Π_γ, which are a sequence of closings and openings by reconstruction, respectively. The MP can be formally defined by

$$\mathrm{MP}(f) = \Pi_i : \left\langle \begin{array}{llll} \Pi_i = \Pi_{\phi_\lambda}, & \text{with} & \lambda = (n-1+i), & \forall \lambda \in [1,n]; \\ \Pi_i = \Pi_{\gamma_\lambda}, & \text{with} & \lambda = (i-n-1), & \forall \lambda \in [n+1, 2n+1]. \end{array} \right. \tag{3}$$

Thus, both the opening and closing profiles are computed with a SE of fixed shape and increasing size. The MP is effective for investigating the interaction of the structures present in the image (i.e. objects in the surveyed scene) with the SE considered. According to its definition, a MP can only handle a scalar image (e.g. one band).

2.2 *Extended morphological profiles*

EMPs (Benediktsson *et al.* 2005) straightforwardly generalize the MP to hyperspectral data. The multi-variate domain of the data is reduced to few dimensions with a PCA (Benediktsson *et al.* 2005). The features extracted by the transformation (i.e. eigenvectors ordered increasingly according to the values of the correspondent eigenvalues), called principal components (PCs), are meaningful for representation since

they account most of the variance of the data in the original feature space. Thus, only the first PCs are considered for the analysis, while the others are discarded. As a general guideline, the number of the considered PCs should contain about 99% of the total variance of the data. Subsequently, on each of the PCs, a full MP is computed. Thus, the EMP of c PCs can be formalized by:

$$\mathrm{EMP} = \{\mathrm{MP(PC_1)}, \mathrm{MP(PC_2)}, \dots, \mathrm{MP(PC_c)}\}. \tag{4}$$

Although the EMP was successfully used for including the spatial information in the classification of HR hyperspectral images, some drawbacks can be pointed out. The main shortcomings of EMPs can be identified as: (i) the limitation given by the operators used for modelling the spatial information; (ii) the feature-extraction technique considered for reducing the dimensionality of the original feature space; and (iii) the increase in the number of features produced by the morphological transformations.

The first drawback mainly resides in the limited flexibility of the operators by reconstruction based on a SE in extracting informative features suitable to model the spatial characteristics of the objects. Obviously, a limitation in the capability of describing spatial features leads directly to a reduction in the discrimination power of the analysis. This drawback is addressed by the present work. The second limitation is related to the transformation used for reducing the dimensionality of the data prior to the morphological processing. The EMPs are computed on the few PCs extracted, which are suitable for the representation of the data, but might not be the most discriminative for classification (Fukunaga 1990, Duda *et al.* 2000). Finally, the issue of the increase of the dimension of the feature space due to the computation of the EMP can be addressed again by applying some feature-extraction techniques, as already presented by Benediktsson *et al.* (2003) and Benediktsson *et al.* (2005).

3. Extended profiles with attribute filters

In this section, the proposed extension of the EMP is presented. At first, the morphological attribute filters and their efficient implementation are presented. Subsequently, the concept of the attribute profile (AP) is briefly recalled. Finally, the proposed filtering techniques for hyperspectral data are defined.

3.1 *Morphological attribute filters*

Morphological attribute filters are connected filters, and the morphological operators by reconstruction are included in their definition (Breen and Jones 1996). They process the input image by removing the connected components that do not fulfil a given criterion. The criterion could evaluate any attribute extracted from the regions. The great flexibility in defining the attribute leads to an improved capability in modelling the spatial information with respect to operators based on fixed SEs. In fact, the attributes considered can be purely geometric (e.g. area, length of the perimeter, image moments, shape factors), textural (e.g. range, standard deviation, entropy), etc. Actually, an attribute can be any measure computable on the regions of the connected components present in the image. However, the attribute criteria may not be increasing. There are two consequences of this drawback. Firstly, such binary criteria do not extend straight to grey-scale images, and secondly, when the parameter of a criterion increases, it may generate a sequence of filters that are not increasingly coarser (i.e. leading to greater simplifications of the image), as actually happens when

increasing the sizes of the SEs in openings and closings by reconstruction. The first point is treated in this section, the second one in §3.3.

Let us consider a numerical function f and a binary criterion T that acts on the sections $h_k(f)$ of f at successive thresholds $k_1 < k_2 < k_3$. We may have $Th_{k_2}(f) = \phi$, whereas $Th_k(f) \neq \phi$ for $k = k_1, k_3$. The successive transformations do not decrease as k increases. Therefore they cannot be considered as the stack of sections of a function. The simplest way to force the decreasingness of the sequence is to replace the transform $Th_k(f)$ by the union of all the transforms from the top section, i.e. by $T * h_k(f) = \cup\{Th_p(f), p \geq k\}$, which is equal to the section at level k of the function transform $\gamma^T(f)$,

$$\gamma^T(f)(x) = \max\{k : x \in Th_k(f)\}. \tag{5}$$

Analogously, as a dual counterpart, the grey-scale thickening transformation can be formulated by:

$$\phi^T(f)(x) = \min\{k : x \in Th_k(f)\}. \tag{6}$$

However, other extensions of binary thinning and thickening to numerical images are possible, leading to different filtering effects (Salembier *et al.* 1998, Urbach *et al.* 2007).

3.2 Max-trees and min-trees

Attribute filters computed on grey-level images according to the definitions in equations (5) and (6) are not efficient in terms of implementation. Instead, they can be efficiently computed on the max-tree representation of the image (Salembier *et al.* 1998). An example of a max-tree is shown in figure 1. An image can be seen as a composition of connected flat regions (i.e. connected components) where all the pixels that belong to one of those regions have the same grey-level value (see figure 1(*b*)). The max-tree maps each of all the connected components of the image to a node organized in a hierarchical tree structure (see figure 1(*c*)). The tree grows from the root, which represents the whole image at its lowest grey-level, to the leaf nodes that correspond to the regional maxima. The tree is created according to a flood-filling algorithm that permits the detection of the connected regions and creates the hierarchical links between the nodes. While a node in the tree represents a set of connected pixels in the image, if it is considered with its descendants also, it represents a peak. This includes all the connected components, contained by the node, made up by pixels with a greater grey-level value. The computation of the attribute filters on the max-tree structure is composed of three steps: (i) max-tree creation; (ii) evaluation of the criterion; and (iii) image restitution. The first step aims at representing the image in the tree structure and it is the phase that is computationally most demanding. The attributes that can be computed incrementally can be calculated during this phase. The second phase performs the evaluation of the criterion. On each node, the attribute required by the criterion is computed and evaluated against a value (λ), which is considered as reference and defines the degree of filtering. The nodes that do not satisfy the criterion are removed while the others are preserved. The pruning of the tree can be done according to different filtering rules (Salembier *et al.* 1998), which only differs in their results if the transformation is not increasing. As presented in Urbach *et al.* (2007), the subtractive rule proved to be the most suitable when considering attributes that are not increasing, such as the image moments. The final
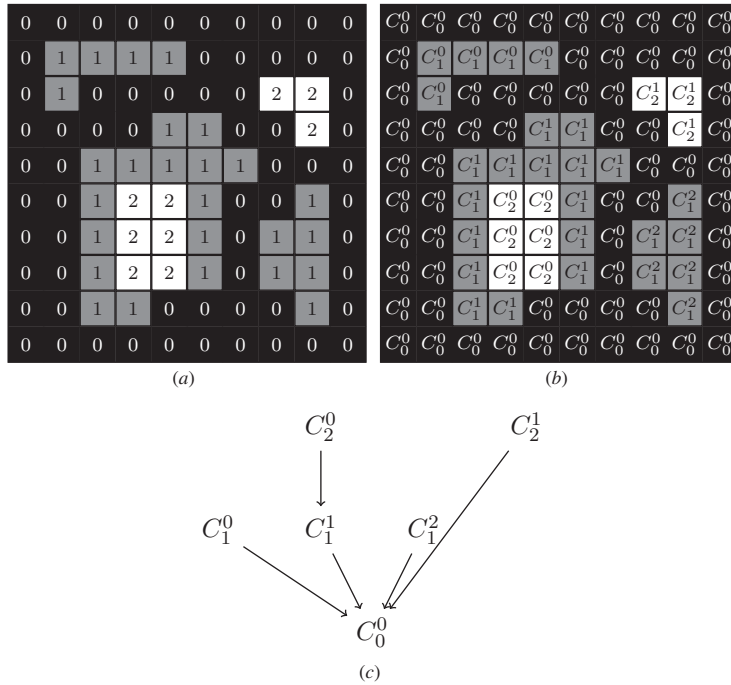
Figure 1. Example of a max-tree. (*a*) Grey-scale image with intensities ranging from 0 to 2; (*b*) image in (*a*) with its connected components labelled and (*c*) max-tree of (*a*). This shows the relations between the nodes associated with the connected components in (*b*).

step simply generates the output image from the pruned tree. The max-tree structure is suitable for anti-extensive transformations (i.e. opening and thinning). For the extensive operators, such as closing and thickening, the min-tree is considered. A min-tree is the representation of the image dual with respect to max-tree, and can be simply computed as the max-tree of the complement of the input image.

3.3 *Attribute profiles*

APs are a multi-level decomposition of the input image based on attribute filters (Dalla Mura *et al.* 2010). As for MPs, APs have to be cumulative functions. This is an important condition because it leads to achieving a progressively increased simplification of the image when the filters values are increased. In the case of openings by reconstruction, it occurs automatically when the size of the SE increases. When considering attribute filters, it is only verified for increasing criteria. Thus, in order to guarantee this property for all attribute filters, the family of criteria T_i taken into account must be formally ordered, so that $i \leq j \Rightarrow T_i \subseteq T_j \Rightarrow \gamma^{T_i} \geq \gamma^{T_j}$. This is different from the increasingness property, which involves two input functions and one criterion, i.e. $f \leq g \Rightarrow \gamma^T(f) \leq \gamma^T(g)$ (a condition which is not fulfilled for thickening and thinning transformations).

Analogously to the MP, the AP can be defined as a concatenation of a thickening AP, $\Pi_{\phi^{T'}}$, and a thinning AP, $\Pi_{\gamma^{T'}}$:

$$\text{AP}(f) = \Pi_i : \begin{cases} \Pi_i = \Pi_{\phi^{T'_\lambda}}, & \text{with} \quad \lambda = (n-1+i), \quad \forall \lambda \in [1, n]; \\ \Pi_i = \Pi_{\gamma^{T'_\lambda}}, & \text{with} \quad \lambda = (i-n-1), \quad \forall \lambda \in [n+1, 2n+1]. \end{cases} \tag{7}$$

Being $T' = \{T_1, T_2, \ldots, T_n\}$ the set of ordered criteria, for $T_i, T_j \in T'$ and $j \geq i$ the relation $T_i \subseteq T_j$ holds.

According to the attribute considered, different information can be extracted from the image. For example, if an increasing attribute is considered (e.g. the area of the regions) the AP performs analysis based on the scale of the structures in the scene. Instead, if a measure of the homogeneity of the grey-level values of the pixels (which is, usually, non-increasing) belonging to each region is considered as an attribute, it is possible to gather information on the texture.

3.4 *Extended attribute profiles and Extended multi-attribute profiles*

Analogously to the definition of EMPs, we can compute the APs on the c PCs extracted from the original hyperspectral data. This leads to the definition of the EAP:

$$\text{EAP} = \{\text{AP}(\text{PC}_1), \text{AP}(\text{PC}_2), \ldots, \text{AP}(\text{PC}_c)\}. \tag{8}$$

We remind the reader that the EAP includes in its definition the EMP (because the operators by reconstruction can be viewed as a particular set of morphological attribute filters) and, thus, it can be considered as its generalization. The main advantage in using the EAP instead of the EMP relies on the great flexibility given by the definition of the attributes used in the processing for modelling the spatial features that need to be extracted. Moreover, the computation of the filters on the max-tree structure reduces the computational complexity with respect to the EMP because the tree (both max- and min-) is built once for each PC and filtered multiple times according to the required number of levels. Samples of EAPs created on different attributes are presented in figure 2. From the figure, it is possible to notice how the thickening and thinning transformations computed with different attributes process the original images in different ways. In particular, one can observe how the profiles built with the area and the length of the diagonal attributes perform differently, even if both the attributes are increasing. When considering the EAP with moment of inertia, it is possible to observe how the effect of the filtering is significantly different from those of the other EAPs. In this profile the elongated structures are revealed. The profile with the standard-deviation attribute also performs differently from the others. For example, one can see that the processing preserves some small regions of high contrast that are instead erased in the other attributes.

Moreover, since APs are created by different attributes to extract different information from the scene, the idea of the EAPs is further evolved to the EMAPs. The EMAP merges different EAPs in a single data structure. An EMAP composed of m different EAPs can be easily formulated as:

$$\text{EMAP} = \{\text{EAP}_{a_1}, \text{EAP}'_{a_2}, \ldots, \text{EAP}'_{a_m}\}, \tag{9}$$

where a_i is a generic attribute and $\text{EAP}' = \text{EAP} \backslash \{\text{PC}_1, \ldots, \text{PC}_c\}$. The latter relation is necessary for avoiding the multiple presence of the c PCs (we remember that $\text{AP}_{a_1, i}(f) = \text{AP}_{a_2, i}(f) = \ldots = \text{AP}_{a_m, i}(f) = f$ for the level $i = n+1$).

It is clear that, although the EMAP leads to an increase in the dimensionality of the features, it gains greater capabilities in extracting spatial information with respect to a single EAP. Moreover, the load in the computation required by an EMAP is slightly

$\phi^T(\text{PC}_1)$ PC$_1$ $\gamma^T(\text{PC}_1)$ $\phi^T(\text{PC}_2)$ PC$_2$ $\gamma^T(\text{PC}_2)$

$\overleftrightarrow{\hspace{3cm}}$ AP(PC$_1$) $\overleftrightarrow{\hspace{3cm}}$ AP(PC$_2$) $\overleftrightarrow{\hspace{3cm}}$
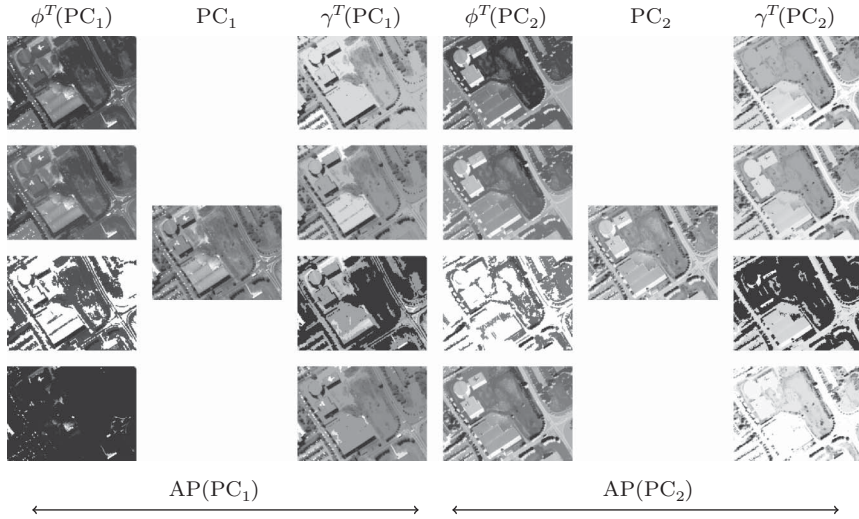
Figure 2. Examples of EAPs computed on the first two PCs of a portion of the University dataset. Each row shows an EAP built by different attributes. Attributes, starting from the first row, are: area, length of the diagonal of the bounding box, moment of inertia and standard deviation. Each EAP is composed by the concatenation of two APs computed on PC$_1$ and PC$_2$. Each AP is made up of three levels, a thickening image ϕ^T, the original PC and a thinning image γ^T. All the thickening and thinning transformations were computed with the following attributes value, λ: area: 5000; length of the diagonal: 100; moment of inertia: 0.5; standard deviation: 50.

greater than that of a single EAP, since the max- and min-tree are computed only once for each PC, and they are filtered with different attributes at different levels. (A MATLAB application for computing the EAP is available on request.)

4. Experimental results

4.1 *Pavia dataset*

The experiments were carried out on two widely used datasets acquired on the city of Pavia, Italy (for a review of work carried out on these images, see Huang and Zhang (2009)). The surveyed scenes are urban areas: one set was acquired on a portion of the city centre, while the other shows the University area. The data were acquired by the hyperspectral airborne sensor ROSIS-03 (Reflective Optics Systems Imaging Spectrometer). The sensor acquired 115 spectral bands, ranging from 0.43 μm to 0.86 μm and the geometrical resolution of the images was 1.3 m. The considered data were atmospherically corrected but not geometrically corrected (e.g. it is possible to notice the geometrical distortions due to the displacement of the airborne platform during the acquisition). The first dataset, which represents the highly dense city centre (in the following referred to as Centre), is a 1096 × 489 pixels portion of the original imaged scene. For this dataset, 102 bands out of the 115 were considered due to noise. Nine thematic classes were considered: water, tree, meadow, self-blocking bricks, soil, asphalt, bitumen, tile and shadow. The image acquired over the University area is composed of 103 bands (12 bands were removed due to noise) of 610 × 340 pixels. Nine thematic classes were identified in this scene: trees, asphalt, bitumen, gravel,

Table 1. Number of samples per class for the train and test sets for the Centre and University datasets.

Class	Centre		University	
	Train	Test	Train	Test
Water	745	65278	–	–
Trees	785	6508	524	3064
Meadow	797	2905	540	18649
Metal sheets	–	–	265	1345
Gravel	–	–	392	2099
Bricks	485	2140	514	3682
Bare Soil	820	6549	532	5029
Asphalt	678	7585	548	6631
Bitumen	808	7287	375	1330
Tiles	223	3122	–	–
Shadow	195	2165	231	947
Total	5536	103539	3921	42776

metal sheets, shadows, self-blocking bricks, meadows and bare soil. The train and test sets for the two datasets are shown in table 1. The true-colour images and the related reference maps are shown in figure 3.

4.2 *Experimental set-up*

For the three datasets, the first four PCs were initially considered in the analysis in order to explain more than the 99% of the total variance of the multi-variate original data. Table 2 reports the values of variance and cumulative variance accounted by the PCs for each dataset.

An EMP with four levels (i.e. leading to a stack of 36 features, 9 for each PC) was computed with a disk-shaped SE of radius increased with a step size of 2. Four attributes were considered in the analysis:
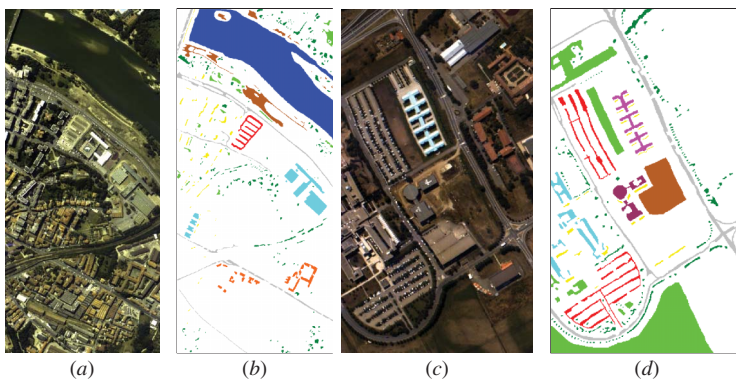

| (*a*) | (*b*) | (*c*) | (*d*) |

Figure 3. True-colour images and maps of the test sets for (*a*)–(*b*) the Centre and (*c*)–(*d*) the University datasets.
Thematic classes for the Centre: ■ water, ■ trees, ☐ asphalt, ■ self-blocking bricks, ☐ bitumen, ■ tiles, ☐ shadows, ■ meadows, ■ bare soil. Thematic classes for the University: ■ trees, ☐ asphalt, ■ bitumen, ☐ gravel, ■ metal sheets, ☐ shadows, ■ meadows, ■ self-blocking bricks, ■ bare soil.

Table 2. Variance (var.) and cumulative variance (cum. var.) explained by each PC for Centre and University datasets.

	Centre		University	
	Var. (%)	Cum. var. (%)	Var. (%)	Cum. var. (%)
PC_1	68.15	68.15	58.32	58.32
PC_2	28.70	96.86	36.10	94.42
PC_3	2.28	99.14	4.44	98.86
PC_4	0.32	99.46	0.30	99.16

(i) a, area of the regions;
(ii) d, diagonal of the box bounding the region (as the area, it is a measure of the size of the regions);
(iii) i, first moment invariant of Hu (1962), or moment of inertia (it measures the elongation of the regions); and
(iv) s, standard deviation of the grey-level values of the pixels in the regions (index related to the homogeneity of the regions).

For each attribute, an EAP was computed. The values of λ used in the filtering are:

(i) EAP_a: $\lambda_a = [100\ 500\ 1000\ 5000]$;
(ii) EAP_d: $\lambda_d = [10\ 25\ 50\ 100]$;
(iii) EAP_i: $\lambda_i = [0.2\ 0.3\ 0.4\ 0.5]$; and
(iv) EAP_s: $\lambda_s = [20\ 30\ 40\ 50]$.

The features obtained by the computation of the four EAPs were also used for creating an EMAP, thus, based on EAP_a, EAP_d, EAP_n and EAP_s.

The original PCs and the extended profiles were analysed by an RF classifier. A RF is an ensemble of decision trees (Breiman 2001). In the learning phase of the classifier, each decision tree is trained with a bootstrapped portion of the training set (the samples left out are used for an internal measure of accuracy, called out-of-bag) and selecting a fraction of the available features for defining the split of each node of the tree. The classification of a pattern is achieved by predicting the class label by each tree in the forest and associating the pattern to the class that gathers most of the votes. In the experiments carried out, a RF was composed of an ensemble of 100 trees, which, in preliminary experiments, showed to be a good trade-off between the accuracy in modelling the problem and the time needed for the learning phase. The number of variables (i.e. features) involved in the training of the classifier was set to the square root of the number of input variables, as suggested by Breiman (2001) as a default value. The accuracy of the obtained results was assessed according to the available test sets by measuring the overall accuracy (OA), the average accuracy (AA) (which is computed as the average of the producer accuracies) and the Kappa coefficient (K). In order to avoid redundancy in the next subsections, only the OA will be discussed. However, the results for AA and K are reported in the tables.

4.3   *Results with extended profiles*

The results obtained by the analysis carried out on the two datasets proved that the inclusion of features that model the spatial information (e.g. those computed by

Table 3. Centre dataset: overall accuracy (OA), average accuracy (AA) and Kappa value of the obtained results. The best accuracies obtained are marked in bold.

Features	PCs 4	EMP 36	EAP_a 36	EAP_d 36	EAP_n 36	EAP_s 36	EMAP 132
OA (%)	96.60	98.27	98.37	98.04	97.97	98.77	**98.83**
AA (%)	93.24	97.66	97.91	96.74	96.43	97.58	**98.02**
Kappa	0.94	0.97	0.97	0.97	0.97	0.98	**0.98**

Table 4. University dataset: overall accuracy (OA), average accuracy (AA) and Kappa value of the obtained results. The best accuracies obtained are marked in bold.

Features	PCs 4	EMP 36	EAP_a 36	EAP_d 36	EAP_n 36	EAP_s 36	EMAP 132
OA (%)	70.42	80.71	**92.32**	86.84	76.24	78.68	89.89
AA (%)	79.25	86.64	**92.00**	88.00	84.68	86.27	90.25
Kappa	0.63	0.75	**0.90**	0.82	0.70	0.73	0.87

extended profiles) can significantly improve the classification accuracies (up to 21.9% for the University dataset) with respect to considering only the spectral information given by the PCs. For this reason, the results obtained by the PCs alone are reported, but they will not be further discussed.

For the Centre dataset, analogous conclusions can be drawn. In general, the results obtained by all the experimental configurations were very good (OA ranging from 96.6% to 98.83%). However, the best accuracies were obtained by the EMAP (see table 3). The gain with respect to the single PCs and the EMP was about 2.2% and 0.6%. It is possible to notice how the accuracies obtained by the EMP are similar to those obtained by the EAPs.

In comparison to the Centre dataset, different results were obtained for the University dataset (table 4). The EAP built by the area attribute performed the best for the University dataset, with a relative increase of OA of about 2.4% and 11.6% as compared to the EMAP and EMP, respectively. The other EAPs performed similarly to the EMP ($\sim\pm5\%$) and worse than the EMAP in terms of accuracies (at minimum, -3% obtained by EAP_d). The motivation of the worst performance of the EMAP with respect to the EAP_a could be due to the great difference of the dimensionality of the features generated by the two operators (36 for the EAP versus 132 for the EMAP).

Tables 5 and 6 report the class-specific accuracies (producer and user accuracies) for the three datasets.

Details of the classification maps obtained for the two datasets are shown in figures 4 and 5. Although it is not possible to clearly indicate which types of objects in the scene benefit from the use of a specific attribute in the classified images, it is clear that the information extracted by the EAPs leads to an overall increase in the precision of the maps.

4.4 *Experiments with a reduced number of PCs*

In order to better investigate the behaviour of extended profiles in extracting informative features, we carried out some experiments with a reduced number of PCs. Tables 7 and 8 report the results in terms of OA, AA and Kappa coefficient, respectively, for the extended profiles computed on the first 3, 2 and 1 PCs. The

Table 5. Centre dataset: class-specific producer accuracy (PA) and user accuracy (UA) of the obtained results. The best accuracies obtained are marked in bold.

	PCs		EMP		EAP$_a$		EAP$_d$		EAP$_n$		EAP$_s$		EMAP	
	PA (%)	UA (%)	PA (%)	UA (%)	PA (%)	UA (%)	PA (%)	UA (%)	PA (%)	UA (%)	PA (%)	UA (%)	PA (%)	UA (%)
Water	98.83	**100.00**	98.87	**100.00**	98.87	**100.00**	98.89	**100.00**	98.86	**100.00**	**100.00**	**100.00**	99.59	**100.00**
Trees	88.60	97.42	93.53	97.81	91.50	97.54	92.09	97.07	**94.15**	97.24	90.07	**97.94**	91.43	97.69
Meadow	94.60	77.19	95.18	86.70	94.60	83.37	93.60	84.49	94.18	**86.77**	**95.59**	80.99	94.94	83.55
Bricks	76.17	80.93	97.43	98.63	**99.39**	99.39	92.06	99.04	88.50	96.68	99.25	99.48	99.30	**99.58**
Bare Soil	95.02	94.45	99.73	99.50	99.77	99.88	99.68	98.40	98.98	96.52	99.73	**99.91**	**99.79**	**99.91**
Asphalt	93.43	90.70	97.17	**96.26**	**99.71**	90.29	97.94	89.00	97.21	92.45	99.26	94.61	99.39	94.26
Bitumen	92.95	89.57	97.19	92.25	97.46	98.11	96.57	97.64	96.24	97.91	94.41	99.26	**97.80**	**99.65**
Tiles	99.65	91.50	99.90	91.44	99.94	99.49	99.90	95.88	99.81	87.19	99.90	**99.97**	**99.97**	99.21
Shadow	99.91	**100.00**	99.91	**100.00**	99.95	**100.00**	99.95	**100.00**	99.91	**100.00**	**100.00**	**100.00**	99.95	**100.00**

Table 6. University dataset: class-specific producer accuracy (PA) and user accuracy (UA) of the obtained results. The best accuracies obtained are marked in bold.

|	PCs		EMP		EAP_a		EAP_d		EAP_n		EAP_s		EMAP	
	PA (%)	UA (%)	PA (%)	UA (%)	PA (%)	UA (%)	PA (%)	UA (%)	PA (%)	UA (%)	PA (%)	UA (%)	PA (%)	UA (%)
Asphalt	77.54	91.49	91.84	96.18	**94.60**	**99.90**	93.27	99.74	91.28	98.94	93.49	99.41	**94.60**	99.75
Meadow	57.50	90.19	72.66	89.34	**95.60**	**92.94**	90.99	86.59	66.16	86.44	70.27	86.94	93.82	89.56
Gravel	49.74	60.45	**70.84**	88.46	67.65	95.75	65.51	92.41	53.36	87.43	61.79	90.19	67.84	**96.35**
Trees	99.05	51.39	99.28	71.83	98.96	**79.14**	**99.41**	68.63	99.31	51.58	98.17	45.51	99.15	73.86
Metal sheets	99.33	93.75	99.55	97.67	99.41	**100.00**	99.26	**100.00**	**99.63**	98.24	98.74	85.24	98.96	99.48
Bare soil	**74.49**	41.57	67.29	45.67	73.39	**97.03**	47.35	85.19	58.66	45.00	56.53	58.31	59.30	94.58
Bitumen	69.40	63.18	82.03	96.98	99.77	100.00	98.42	98.72	99.85	99.92	99.92	100.00	**100.00**	**100.00**
Bricks	88.08	67.65	98.07	**79.91**	**98.72**	79.37	97.80	77.61	95.19	69.83	97.94	76.72	98.56	79.24
Shadow	98.10	98.62	98.20	99.36	99.89	99.27	**100.00**	98.85	98.63	**99.89**	99.58	98.74	**100.00**	98.85
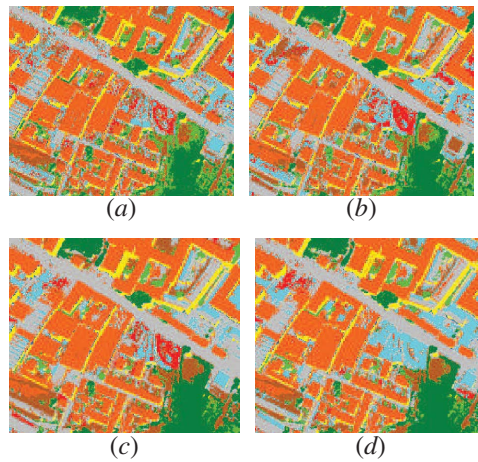
Figure 4. Centre dataset. Details of the classification maps obtained by: (*a*) the PCs, (*b*) the EMP, (*c*) the EAP$_a$ and (*d*) the EMAP.
Thematic classes: ▇ water, ▇ trees, ▇ asphalt, ▇ self-blocking bricks, ▇ bitumen, ▇ tiles, ▇ shadows, ▇ meadows, ▇ bare soil.
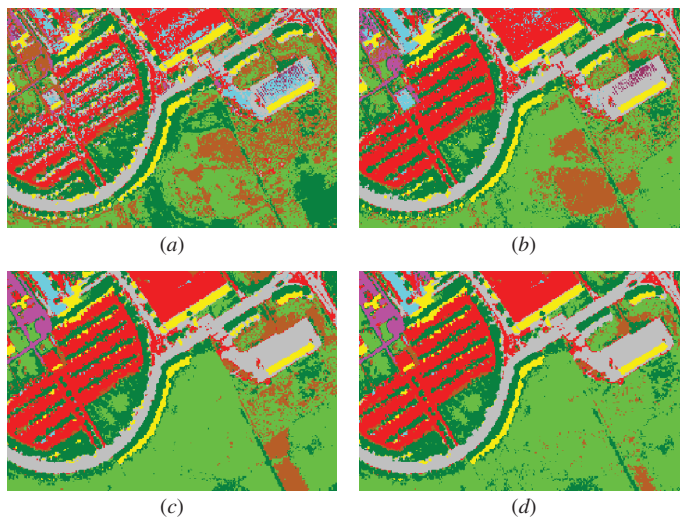
Figure 5. University dataset. Details of the classification maps obtained by: (*a*) the PCs, (*b*) the EMP, (*c*) the EAP$_a$ and (*d*) the EMAP.
Thematic classes: ▇ trees, ▇ asphalt, ▇ bitumen, ▇ gravel, ▇ metal sheets, ▇ shadows, ▇ meadows, ▇ self-blocking bricks, ▇ bare soil.

most notable trend in all the experiments is the steep increase in the accuracy when considering only the first PC and the first two PCs. Concerning the relative overall accuracies obtained by the different extended profiles, we can state that for the centre datasets, the EMAP always performed the best in terms of accuracies, except when considering the first two PCs where the best results were obtained by EAP$_s$ (−0.31%) for the Centre dataset.

Table 7. Centre dataset: overall accuracy (OA), average accuracy (AA) and Kappa value obtained by considering a reduced number of PCs. The best accuracies obtained are marked in bold.

		PCs	EMP	EAP_a	EAP_d	EAP_n	EAP_s	EMAP
OA (%)	PC_{1-3}	95.99	97.92	98.47	98.16	97.95	98.81	**98.96**
	PC_{1-2}	93.57	96.81	97.95	97.44	97.78	**98.57**	98.26
	PC_1	51.48	66.41	88.57	86.79	91.36	93.37	**94.24**
AA (%)	PC_{1-3}	91.89	96.42	98.26	97.34	96.64	97.61	**98.45**
	PC_{1-2}	85.87	94.17	97.31	96.00	96.19	97.03	**97.72**
	PC_1	41.97	61.25	80.46	70.49	79.88	85.71	**88.46**
Kappa	PC_{1-3}	0.93	0.96	0.97	0.97	0.97	0.98	**0.98**
	PC_{1-2}	0.89	0.95	0.97	0.96	0.96	**0.98**	0.97
	PC_1	0.35	0.52	0.81	0.77	0.85	0.89	**0.90**

Table 8. University dataset: overall accuracy (OA), average accuracy (AA) and Kappa value obtained by considering a reduced number of PCs. The best accuracies obtained are marked in bold.

		PCs	EMP	EAP_a	EAP_d	EAP_n	EAP_s	EMAP
OA (%)	PC_{1-3}	64.94	76.62	**90.54**	79.66	73.22	75.99	88.77
	PC_{1-2}	61.17	72.69	**88.18**	80.31	71.04	81.25	86.96
	PC_1	38.73	46.21	55.34	48.62	44.80	48.23	**63.16**
AA (%)	PC_{1-3}	75.44	86.73	**91.03**	86.04	83.43	85.31	90.43
	PC_{1-2}	72.21	83.86	88.16	85.94	81.43	85.34	**88.23**
	PC_1	50.57	64.08	69.08	64.52	60.52	65.82	**73.20**
Kappa	PC_{1-3}	0.57	0.71	**0.87**	0.74	0.67	0.70	0.85
	PC_{1-2}	0.53	0.66	**0.84**	0.75	0.64	0.76	0.83
	PC_1	0.26	0.37	0.47	0.38	0.34	0.39	**0.55**

When considering the University dataset, by decreasing the number of considered PCs a trend in the difference of OA between the EAP_a and the EMAP is noticed. The improvement in OA of the EAP_a over the EMAP is 2.4% with four PCs (see § 4.3). This difference decreases with the reduction of the number of PCs. In contrast, when considering only one PC, the OA obtained by the EMAP exceeds the one of EAP_a by 7.8%.

From this set of experiments, it is possible to conclude that with a reduced number of PCs (i.e. with a reduced number of features generated by the profiles), the EMAP outperforms the other extended profiles, in terms of overall accuracies.

5. Conclusion

In this paper, EAPs and EMAPs have been proposed for the analysis of high-resolution hyperspectral images. The introduced extended profiles are based on morphological attribute filters, which have already proven their suitability to the analysis of high-resolution images. In particular, this work aims at exploiting the great flexibility in defining the attributes (and thus, in modelling the features related to the chosen attributes), which is provided by this set of morphological operators.

The extended profiles proposed in this work follow the architecture of the previously proposed EMPs. In greater detail, the attribute filters are applied to a subset of the first PCs extracted from the original data and then concatenated into a single

data structure. EAPs are based on a multi-level analysis of the PCs based on a single attribute. In contrast, the extended multi-attribute profiles take into account multiple attributes. On the one hand, this leads to an increase in the dimensionality of the extracted features; on the other hand, this results in a greater and more precise modelling of the spatial features.

The proposed techniques were applied to two high-resolution hyperspectral images acquired over the city of Pavia, Italy. The datasets represent a portion of the dense urban centre of the city and a University area. Four attributes were considered in the analysis, leading to the generation of four correspondent EAPs: (i) area; (ii) diagonal of the bounding box; (iii) moment of inertia; and (iv) standard deviation. The obtained profiles were also combined together in an EMAP. The features extracted by the extended profiles were considered for classification by an RF classifier. The single PCs and the features generated by a conventional EMP were considered for comparison. From the obtained results, it is possible to make the observation that the proposed extended profiles led to better classification accuracies than those generated by both the PCs alone and the EMP. This result can be explained by the better capability of the extended profiles based on attribute filters in describing spatial features than the conventional approach based on the extended morphological profile. By analysing the results obtained by the proposed extended profiles, it is possible to notice that the classification of multiple attributes achieved the best accuracies for the dataset of the centre. Conversely, on the University dataset, the EAP with area attribute outperformed the others. This can be due to the significant increase in the dimensionality of the features generated by the EMAP with respect to the single EAPs, which may affect the generalization capabilities of the classifier.

For future developments, we aim to investigate the reduction of the high dimensionality of the features extracted by the extended profiles (especially when considering multiple attributes) with proper feature-extraction techniques.

References

BENEDIKTSSON, J.A., PALMASON, J.A. and SVEINSSON, J.R., 2005, Classification of hyperspectral data from urban areas based on extended morphological profiles. *IEEE Transactions on Geoscience and Remote Sensing*, **43**, pp. 480–491.

BENEDIKTSSON, J.A., PESARESI, M. and AMASON, K., 2003, Classification and feature extraction for remote sensing images from urban areas based on morphological transformations. *IEEE Transactions on Geoscience and Remote Sensing*, **41**, pp. 1940–1949.

BREEN, E.J. and JONES, R., 1996, Attribute openings, thinnings, and granulometries. *Computer Visual and Image Understanding*, **64**, pp. 377–389.

BREIMAN, L., 2001, Random forests. *Machine Learning*, **45**, pp. 5–32.

DALLA MURA, M., BENEDIKTSSON, J.A., WASKE, B. and BRUZZONE, L., 2009, Morphological attribute filters for the analysis of very high resolution images. In *Proceedings of the IEEE International Geoscience & Remote Sensing Symposium*, 13–17 July, Cape Town, South Africa, pp. 97–100.

DALLA MURA, M., BENEDIKTSSON, J.A., WASKE, B. and BRUZZONE, L., 2010, Morphological attribute profiles for the analysis of very high resolution images. *IEEE Transactions on Geoscience and Remote Sensing*, **48**, pp. 3747–3762.

DUDA, R.O., HART, P.E. and STORK, D.G., 2000, *Pattern Classification* (New York, NY: Wiley-Interscience Publication).

FAUVEL, M., BENEDIKTSSON, J.A., CHANUSSOT, J. and SVEINSSON, J.R., 2008, Spectral and spatial classification of hyperspectral data using SVMs and morphological profiles. *IEEE Transactions on Geoscience and Remote Sensing*, **46**, pp. 3804–3814.

FUKUNAGA, K., 1990, *Introduction to Statistical Pattern Recognition*, 2nd edn (London, UK: Academic Press).

HU, M.K., 1962, Visual pattern recognition by moment invariants. *IRE Transactions on Information Theory*, **8**, pp. 179–187.

HUANG, X. and ZHANG, L., 2009, A comparative study of spatial approaches for urban mapping using hyperspectral ROSIS – images over Pavia City, northern Italy. *International Journal of Remote Sensing*, **30**, pp. 3205–3221.

JOELSSON, S.R., BENEDIKTSSON, J.A. and SVEINSSON, J.R., 2005, Random forest classifiers for hyperspectral data. In *Proceedings of the IEEE International Geoscience and Remote Sensing Symposium IGARSS 2005*, 1, pp. 25–29.

PALMASON, J.A., BENEDIKTSSON, J.A., SVEINSSON, J.R. and CHANUSSOT, J., 2005, Classification of hyperspectral data from urban areas using morphological preprocessing and independent component analysis. In *Proceedings of the IEEE International Geoscience and Remote Sensing Symposium IGARSS 2005*, 1, pp. 25–29.

PESARESI, M. and BENEDIKTSSON, J.A., 2001, A new approach for the morphological segmentation of high-resolution satellite imagery. *IEEE Transactions on Geoscience and Remote Sensing*, **39**, pp. 309–320.

PLAZA, A., MARTINEZ, P., PEREZ, R. and PLAZA, J., 2002, Spatial/spectral endmember extraction by multidimensional morphological operations. *IEEE Transactions on Geoscience and Remote Sensing*, **40**, pp. 2025–2041.

PLAZA, A., MARTINEZ, P., PLAZA, J. and PEREZ, R., 2005, Dimensionality reduction and classification of hyperspectral image data using sequences of extended morphological transformations. *IEEE Transactions on Geoscience and Remote Sensing*, **43**, pp. 466–479.

PLAZA, A., BENEDIKTSSON, J.A., BOARDMAN, J.W., BRAZILE, J., BRUZZONE, L., CAMPS-VALLS, G., CHANUSSOT, J., FAUVEL, M., GAMBA, P., GUALTIERI, A., MARCONCINI, M., TILTON, J.C. and TRIANNI, G., 2009, Recent advances in techniques for hyperspectral image processing. *Remote Sensing of Environment*, **113**, pp. 5110–5122.

SALEMBIER, P., OLIVERAS, A. and GARRIDO, L., 1998, Antiextensive connected operators for image and sequence processing. *IEEE Transactions on Image Processing*, **7**, pp. 555–570.

SALEMBIER, P. and SERRA, J., 1995, Flat zones filtering, connected operators, and filters by reconstruction. *IEEE Transactions on Image Processing*, **4**, pp. 1153–1160.

SERRA, J., 1988, *Image Analysis and Mathematical Morphology, Theoretical Advances*, Vol. 2 (New York, NY: Academic Press).

SERRA, J., 1983, *Image Analysis and Mathematical Morphology* (New York, NY: Academic Press).

SOILLE, P., 2003, *Morphological Image Analysis, Principles and Applications*, 2nd edn (Berlin, Germany: Springer Verlag).

URBACH, E.R., ROERDINK, J.B.T.M. and WILKINSON, M.H.F., 2007, Connected shape-size pattern spectra for rotation and scale-invariant classification of gray-scale images. *IEEE Transactions on Pattern Analysis and Machine Intelligence*, **29**, pp. 272–285.

ZHU, C., SHI, W., PESARESI, M., LIU, L., CHEN, X. and KING, B., 2005, The recognition of road network from high-resolution satellite remotely sensed data using image morphological characteristics. *International Journal of Remote Sensing*, **26**, pp. 5493–5508.